However, by the use of $a(t) = e^{tH}$, the left hand side of (3.2) can be evaluated using (3.1) to give

$$2\frac{\ddot{a}}{a} + \left(\frac{\dot{a}}{a}\right)^2 = 8\pi G\rho\,. \tag{3.3}$$

In order for (3.2) and (3.3) to agree, the equation of state of matter must be

$$p = -\rho\,. \tag{3.4}$$

Therefore, "new cosmology" (i.e. description of matter in terms of fields) is required in order to obtain inflation.

It is not hard to show that an equation of state like (3.4) with negative pressure can be obtained if matter is described in terms of scalar fields. Consider the Lagrangian $L(\varphi)$ for a theory of a scalar field $\varphi(\underline{x}, t)$:

$$\mathcal{L}(\varphi) = \frac{1}{2}\partial_\mu\varphi\partial^\mu\varphi - V(\varphi)\,. \tag{3.5}$$

Given the Lagrangian, the energy–momentum tensor $T_{\mu\nu}$ can be determined as in any classical field theory (see Ref. 51). In a Universe with FRW metric

$$g_{\mu\nu} = \mathrm{diag}\,(1, -a^2(t), -a^2(t), -a^2(t)) \tag{3.6}$$

we obtain for $\rho = T_{00}$ and $p = \frac{1}{3}\sum_{i=1}^{3} T_{ii}$

$$\begin{aligned} \rho(\underline{x}, t) &= \frac{1}{2}\dot{\varphi}^2(\underline{x}, t) + \frac{1}{2}a^{-2}(\nabla\varphi)^2 + V(\varphi)\,, \\ p(\underline{x}, t) &= \frac{1}{3}\sum_{i=1}^{3} T_{ii} = \frac{1}{2}\dot{\varphi}^2(\underline{x}, t) - \frac{1}{6}a^{-2}(\nabla\varphi)^2 - V(\varphi)\,. \end{aligned} \tag{3.7}$$

Thus, if $\varphi(\underline{x}, t_i) = \text{const}$ and $\dot{\varphi}(\underline{x}, t_i) = 0$ at some initial time t_i and $V(\varphi(\underline{x}, t_i)) > 0$, then the equation of state becomes $p = -\rho$ and leads to inflation.

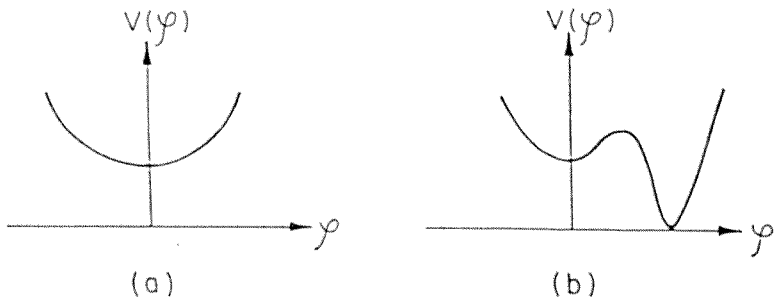

Two examples which give inflation are shown in Fig. 8. In (a), inflation occurs at the stable fixed point $\varphi(\underline{x}, t_i) = 0 = \dot{\varphi}(\underline{x}, t_i)$. However, this model is ruled out by observation: the inflationary phase has no ending. $V(0)$ acts as a permanent nonvanishing cosmological constant. In (b), a finite period of inflation can arise if $\varphi(\underline{x})$ is trapped at the local minimum $\varphi = 0$ with $\dot{\varphi}(\underline{x}) = 0$. However, in this case $\varphi(\underline{x})$ can make a sudden transition at some time $t_R > t_i$ through the potential barrier and move to $\varphi(\underline{x}) = a$. Thus, for $t_i < t < t_R$ the Universe expands exponentially, whereas for $t > t_R$ the contribution of φ to the expansion of the Universe vanishes and we get the usual FRW cosmology. There are two obvious questions: How does the transition occur and why should the scalar field have $V(\varphi) = 0$ at the global minimum? In the following section the first question will be addressed. The second question is part of the cosmological constant problem, for which there is as yet no convincing explanation. Before studying the dynamics of the phase transition, we need to digress and discuss finite temperature effects.

3.2. *Finite temperature field theory*

The evolution of particles in vacuum and in a thermal bath are very different. Similarly, the evolution of fields changes when coupled to a thermal bath. Under certain conditions, the changes may be absorbed in a temperature-dependent potential, the finite temperature effective potential.[52] Here, a heuristic derivation of this potential will be given. (See Ref. 53 or the original articles[52] for the actual derivation.)

We assume that the scalar field $\varphi(\underline{x}, t)$ is coupled to a thermal bath which is represented by a second scalar field $\psi(\underline{x}, t)$ in thermal equilibrium. The Lagrangian for φ is

$$\mathcal{L} = \frac{1}{2}\partial_\mu\varphi\partial^\mu\varphi - V(\varphi) - \frac{1}{2}\hat{\lambda}\varphi^2\psi^2\,, \tag{3.8}$$

where $\hat{\lambda}$ is a coupling constant. The action from which the equations of motion are derived is

$$S = \int d^4x\,\sqrt{-g}\mathcal{L}\,, \tag{3.9}$$

where g is the determinant of the metric (3.6). The resulting equation of motion for $\varphi(\underline{x}, t)$ is

$$\ddot{\varphi} + 3H\dot{\varphi} - a^{-2}\nabla^2\varphi = -V'(\varphi) - \hat{\lambda}\psi^2\varphi\,. \tag{3.10}$$

If ψ is in thermal equilibrium, we may replace ψ^2 by its thermal expectation value $\langle\psi^2\rangle_T$. Now,

$$\langle\psi^2\rangle_T \sim T^2\,, \tag{3.11}$$

which can be seen as follows: in thermal equilibrium, the energy density of ψ equals that of one degree of freedom in the thermal bath. In particular, the potential energy density $V(\psi)$ of ψ is of that order of magnitude. Let

$$V(\psi) = \lambda_\psi\psi^4 \tag{3.12}$$

with a coupling constant λ_ψ, which we take to be of order 1 (if λ_ψ is too small, ψ will not be in thermal equilibrium). Since the thermal energy density is proportional to T^4, (3.11) follows. (3.10) can be rewritten as

$$\ddot{\psi} + 3H\dot{\varphi} - a^{-2}\nabla^2\varphi = -V_T'(\varphi)\,, \tag{3.13}$$

where

$$V_T(\varphi) = V(\varphi) + \frac{1}{2}\hat{\lambda}T^2\varphi^2 \tag{3.14}$$

is called the finite temperature effective potential. Note that in (3.14), $\hat{\lambda}$ has been rescaled to absorb the constant of proportionality in (3.11).

These considerations will now be applied to Example A, a scalar field model with potential

$$V(\varphi) = \frac{1}{4}\lambda(\varphi^2 - \eta^2)^2 \tag{3.15}$$

(η is called the scale of symmetry breaking). The finite temperature effective potential becomes (see Fig. 9)

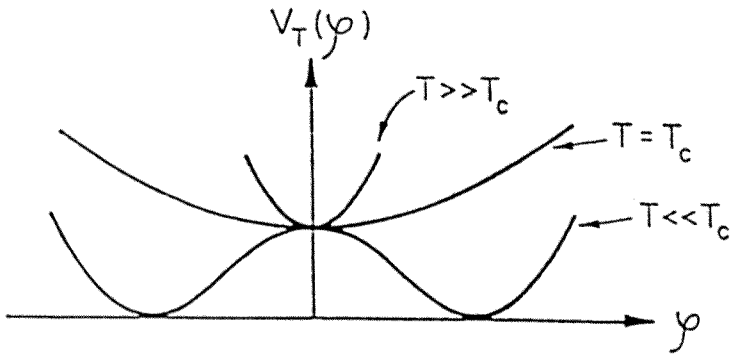

Fig. 9. The finite temperature effective potential for Example A.

$$V_T(\varphi) = \frac{1}{4}\lambda\varphi^4 - \frac{1}{2}\left(\lambda\eta^2 - \hat{\lambda}T^2\right)\varphi^2 + \frac{1}{4}\lambda\eta^4\,. \tag{3.16}$$

For very high temperatures, the effective mass term is positive and hence the energetically favorable state is $\langle\varphi\rangle = 0$. For very low temperatures, on the other hand, the mass term has a negative sign which leads to spontaneous symmetry breaking. The temperature at which the mass term vanishes defines the critical temperature T_c:

$$T_c = \hat{\lambda}^{-1/2}\lambda^{1/2}\eta\,. \tag{3.17}$$

As Example B, consider a theory with potential

$$V(\varphi) = \frac{1}{4}\varphi^4 - \frac{1}{3}(a+b)\varphi^3 + \frac{1}{2}ab\varphi^2 \tag{3.18}$$

with $\frac{1}{2}a > b > 0$. The finite temperature effective potential is obtained by adding $\frac{1}{2}\hat{\lambda}T^2\varphi^2$ to the right hand side of (3.18). $V_T(\varphi)$ is sketched in Fig. 10 for various values of T. The critical temperature T_c is defined as the temperature when the two minima of $V_T(\varphi)$ become degenerate.

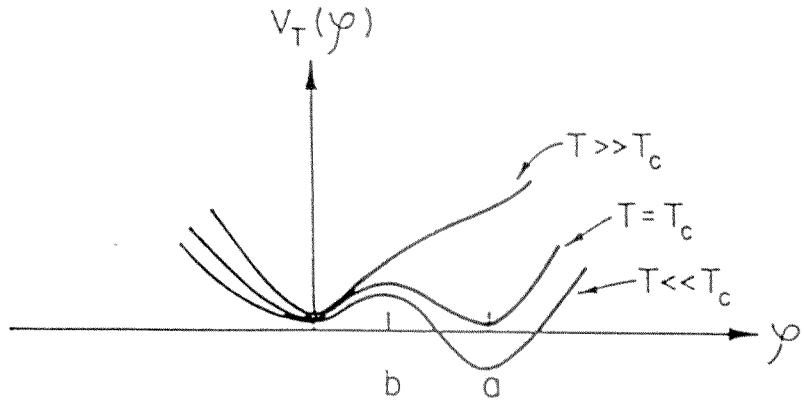

Fig. 10. The finite temperature effective potential for Example B.

It is important to note that the use of finite temperature effective potential methods is legitimate only if the system is in thermal equilibrium. This point was stressed in Refs. 54 and 55, although the fact should be obvious from the derivation given above. To be more precise, we require the ψ field to be in thermal equilibrium and the coupling constant $\hat{\lambda}$ of (3.8), which mediates the energy exchange between the φ and ψ fields, to be large. However (see, for example, Ref. 18), observational constraints stemming from the amplitude of the primordial energy density fluctuation spectrum force the self-coupling constant λ of φ to be extremely small. Since at one-loop order the interaction term $\frac{1}{2}\hat{\lambda}\varphi^2\psi^2$ induces contributions to λ, it is unnatural to have λ very small and $\hat{\lambda}$ unsuppressed. Hence, in many inflationary Universe models — particularly in new inflation[56] and in chaotic inflation[54] — finite temperature effective potential methods are inapplicable.

3.3. *Phase transitions*

The temperature dependence of the finite temperature effective potential in quantum field theory leads to phase transitions in the very early Universe. These transitions are either first or second order.

Example A of the previous section provides a model in which the transition is second order (see Fig. 9). For $T \gg T_c$, the expectation value of the scalar field φ vanishes at all points $\underline{x}$ in space:

$$\langle\varphi(\underline{x})\rangle = 0\,. \tag{3.19}$$

In the following subsections we will construct the various types of defects. Th cosmological implications will be discussed in later sections.

The easiest defect to construct is the domain wall. Consider $n = 1$ [or, mor generally, a theory with $\Pi_0(\mathcal{M}) \neq 1$]. In this case, the vacuum manifold consists o two points:

$$\varphi_{\text{vac}} = \pm\eta \,. \tag{3.44}$$

During the symmetry-breaking phase transition, regions in physical space $\mathcal{R}^3$ wit $\varphi = \pm\eta$ will form. These regions are separated by two-dimensional surfaces (walls with $\varphi \notin \mathcal{M}$ (see Fig. 11). These are the domain walls. Since $\varphi \notin \mathcal{M}$ in th walls, $V(\varphi) > 0$ and hence the walls carry energy per unit area. Via the usua gravitational force, this energy can act as a seed for structures in the Universe.

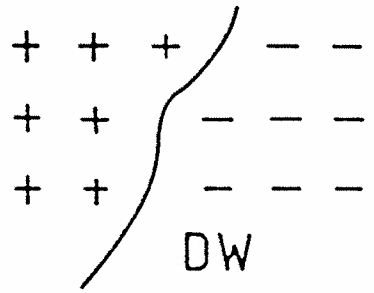

Fig. 11. A two-dimensional cross section through space showing a domain wall (DW) separatin a region with $\varphi = \eta$ (+) from a neighboring region with $\varphi = -\eta$ (−).

3.6. *Cosmic strings*

Consider a theory in which matter consists of a gauge field A_μ and a complex scala field ϕ whose dynamics is given by the Lagrangian

$$\mathcal{L} = \frac{1}{2} D_\mu\phi D^\mu\phi - V(\phi) + \frac{1}{4} F_{\mu\nu}F^{\mu\nu} \,, \tag{3.45}$$

where $F_{\mu\nu}$ is the field strength tensor. The potential $V(\phi)$ has the symmetry-breaking "Mexican hat" shape (see Fig. 12):

$$V(\phi) = \frac{1}{4}\lambda(|\phi|^2 - \eta^2)^2 \,. \tag{3.46}$$

Hence, the vacuum manifold $\mathcal{M}$, the space of minimum energy density configurations, is a circle S^1.

The theory described by (3.45) and (3.46) admits one-dimensional topologica defects, cosmic strings. In the Abelian Higgs model of this example the strin solutions were first found by Nielsen and Olesen.[67] It is possible to construc

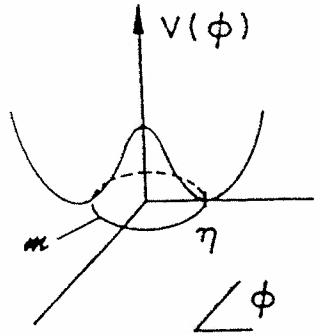

Fig. 12. The zero temperature potential energy of the complex scalar field used in the cosmic string model.

string configurations which are translationally invariant along the z axis. On a circle C in the $x - y$ plane with radius r (see Fig. 13), the boundary conditions for ϕ are

$$\phi(r, \theta) = \eta e^{i\theta} \,, \tag{3.47}$$

where θ is the polar angle along C.

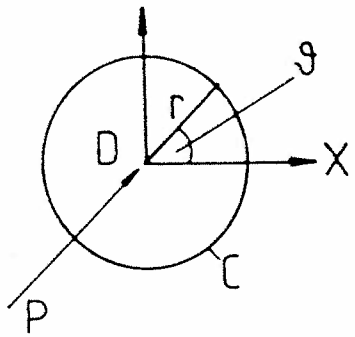

Fig. 13. Sketch of the cosmic string construction of Subsec. 3.6. (See text for notation.)

The configuration (3.47) has winding number 1: at all points of the circle, ϕ takes on values in $\mathcal{M}$, and as φ varies from 0 to 2π, ϕ winds once round $\mathcal{M}$. By continuity it follows that there must be a point p on the disk D bounded by C where $\phi = 0$. By translational symmetry there is a line of points with $\phi = 0$. This line is the center of the cosmic string. The cosmic string is a line of trapped potential energy. In order to minimize the total energy given the prescribed topology (i.e. winding number), the thickness of the string [i.e. radius over which $V(\phi)$ deviates significantly from 0] must be finite. As first shown in Ref. 67, the width w of a string is

$$w \simeq \lambda^{-1/2}\eta^{-1}\,, \tag{3.48}$$

from which it follows that the mass per unit length μ is

$$\mu \simeq \eta^2\,, \tag{3.49}$$

i.e. independent of the self-coupling constant λ.

Cosmic strings arise in any model in which the vacuum manifold satisfies the topological criterion

$$\Pi_1(\mathcal{M}) \neq 1\,. \tag{3.50}$$

Any field configuration $\phi(\underline{x})$ is characterized by an integer n, the element of $\Pi_1(\mathcal{M})$ corresponding to $\phi(\underline{x})$. (Roughly speaking, n can be viewed as the number of times the map φ from C to $\mathcal{M}$ covers $\mathcal{M}$.)

A cosmic string is an example of a *topological defect* has a well-defined core, a region in space where $\phi \notin \mathcal{M}$ and hence $V(\phi) > 0$. There is an associated winding with number, and it is quantized. Hence, a topological defect is stable. Furthermore, topological defects exist for theories with global and local symmetry groups.

3.7. *Monopoles*

If the theory contains three real scalar fields ϕ_i with potential (3.46) (if $|\phi|^2 = \sum_{i=1}^3 \phi_i^2$), then $\Pi_2(\mathcal{M}) \neq 1$ and monopoles result. The construction of a monopole configuration is illustrated in Fig. 14. As the origin in physical space we select a point which is to become the center of the monopole. Consider a sphere S_r of radius r surrounding this point. A spherically symmetric monopole configuration is obtained by the identity map

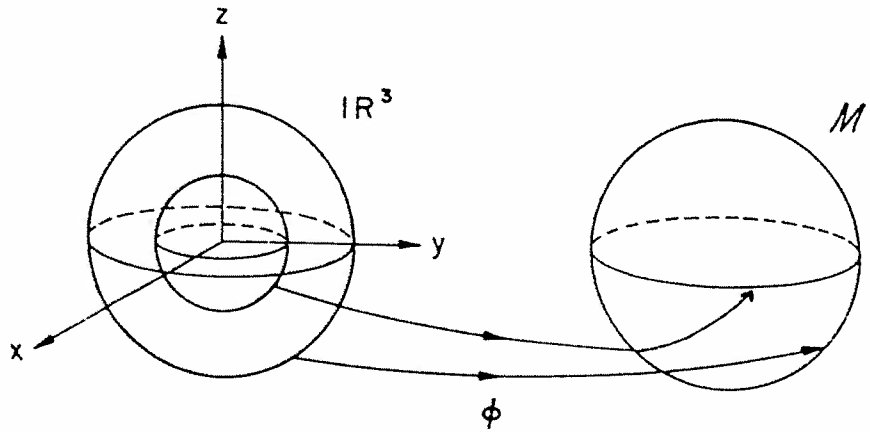

Fig. 14. Construction of a monopole: on the left is physical space, on the right the vacuum manifold. The field configuration ϕ maps spheres in space onto $\mathcal{M}$. However, a core region of space near the origin is mapped onto field values not in $\mathcal{M}$.

$$S_r \to \mathcal{M} = S^2\,, \quad (r,\theta,\varphi) \underset{\varphi}{\to} (\theta,\varphi)\,. \tag{3.51}$$

This configuration has winding number 1. Since the winding number of maps $S^2 \to S^2$ is quantized, it cannot change as r varies. Thus, the only way to obtain a single-valued field configuration at $r = 0$ is for $\varphi(r,\theta,\varphi)$ to leave $\mathcal{M}$ as $r \to 0$. In particular, there is a point (e.g. $r = 0$) for which $\varphi = 0$. This is the center of the monopole. We see that monopoles are topological defects: they contain a core, have quantized winding number and are stable.

3.8. *Global textures*

Next, consider a theory of four real scalar fields given by the Lagrangian

$$\mathcal{L} = \frac{1}{2}\partial_\mu\phi\partial^\mu\phi - V(\phi) \tag{3.52}$$

with

$$V(\phi) = \frac{1}{4}\lambda\left(\sum_{i=1}^{4}\phi_i^2 - \eta^2\right)^2\,. \tag{3.53}$$

In this case, the vacuum manifold is $\mathcal{M} = S^3$ with topology

$$\Pi_3(\mathcal{M}) \neq 1\,, \tag{3.54}$$

and the corresponding defects are the global textures.[1,68,69]

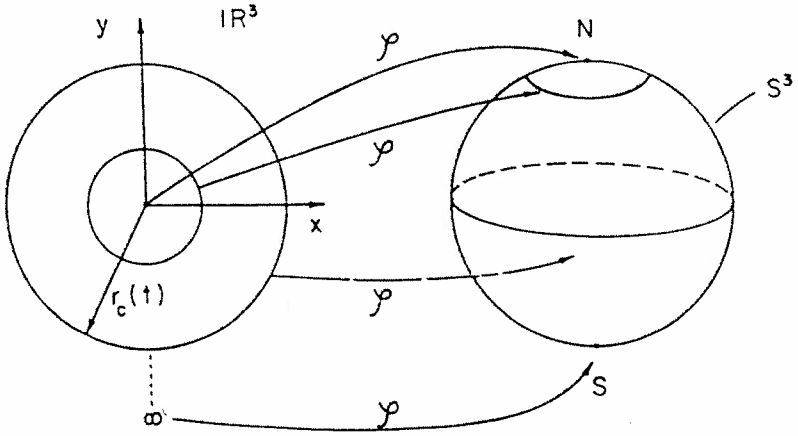

Fig. 15. Construction of a global texture: on the left is physical space, on the right the vacuum manifold. The field configuration ϕ is a map from space to the vacuum manifold (see text).

Textures, however, are quite different than the previous topological defects. The texture construction will render this manifest (see Fig. 15). To construct a radially symmetric texture, we give a field configuration $\phi(x)$ which maps physical space

onto $\mathcal{M}$. The origin 0 in space (an arbitrary point which will be the center of th texture) is mapped onto the north pole N of $\mathcal{M}$. Spheres surrounding 0 are mappe onto spheres surrounding N. In particular, some sphere with radius $r_c(t)$ is mappe onto the equator sphere of $\mathcal{M}$. The distance $r_c(t)$ can be defined as the radius the texture. Inside this sphere, $\phi(x)$ covers half the vacuum manifold. Finally, th sphere at infinity is mapped onto the south pole of $\mathcal{M}$. The configuration $\phi(\underline{x})$ ca be parametrized by[69]

$$\phi(x,y,z) = \left(\cos\chi(r), \sin\chi(r)\frac{x}{r}, \sin\chi(r)\frac{y}{r}, \sin\chi(r)\frac{z}{r}\right) \tag{3.55}$$

in terms of a function $\chi(r)$ with $\chi(0) = 0$ and $\chi(\infty) = \pi$. Note that at all point in space, $\phi(\underline{x})$ lies in $\mathcal{M}$. There is no defect core. All the energy is spatial gradien (and possibly kinetic) energy.

In a cosmological context, there is infinite energy available in an infinite space Hence, it is not necessary that $\chi(r) \to \pi$ as $r \to \infty$. We can have

$$\chi(r) \to \chi_{\max} < \pi \quad \text{as} \quad r \to \infty\,. \tag{3.56}$$

In this case, only a fraction,

$$n = \frac{\chi_{\max}}{\pi} - \frac{\sin 2\chi_{\max}}{2\pi}\,, \tag{3.57}$$

of the vacuum manifold is covered: the winding number n is not quantized. Thi is a reflection of the fact that whereas topologically nontrivial maps from S^3 to S exist, all maps from R^3 to S^3 can be deformed to the trivial map.

Textures in R^3 are unstable. For the configuration described above, the insta bility means that $r_c(t) \to 0$ as t increases: the texture collapses. When $r_c(t)$ microscopical, there will be sufficient energy inside the core to cause $\phi(0)$ to leav $\mathcal{M}$, pass through 0 and equilibrate at $\chi(0) = \pi$: the texture unwinds.

A further difference compared to topological defects: textures are relevant onl for theories with global symmetry. Since all the energy is in spatial gradients, for local theory the gauge fields can reorient themselves such as to cancel the energy:

$$D_\mu \phi = 0\,. \tag{3.58}$$

Therefore, it is reasonable to regard textures as an example of a new class defects, *semitopological defects*. In contrast to topological defects, there is no cor and $\phi(\underline{x}) \epsilon \mathcal{M}$ for all $\underline{x}$. In particular, there is no potential energy. Second, th winding number is not quantized, and hence the defects are unstable. Finally, the exist only in theories with a global internal symmetry.

4. Formation and Evolution of Topological Defects

4.1. *Kibble mechanism*

The Kibble mechanism[1] ensures that in theories which admit topological or semi topological defects, such defects will be produced during a phase transition in th very early Universe.

Consider a mechanical toy model, first introduced by Mazenko, Unruh and Wald[55] in the context of inflationary Universe models, which is useful in understanding the scalar field evolution. Consider (see Fig. 16) a lattice of points on a flat table. At each point, a pencil is pivoted. It is free to rotate and oscillate. The tips of nearest neighbor pencils are connected with springs (to mimic the spatial gradient terms in the scalar field Lagrangian). Newtonian gravity creates a potential energy $V(\varphi)$ for each pencil (φ is the angle relative to the vertical direction). $V(\varphi)$ is minimized for $|\varphi| = \eta$ (in our toy model $\eta = \pi/2$). Hence, the Lagrangian of this pencil model is analogous to that of a scalar field with symmetry-breaking potential (3.46).

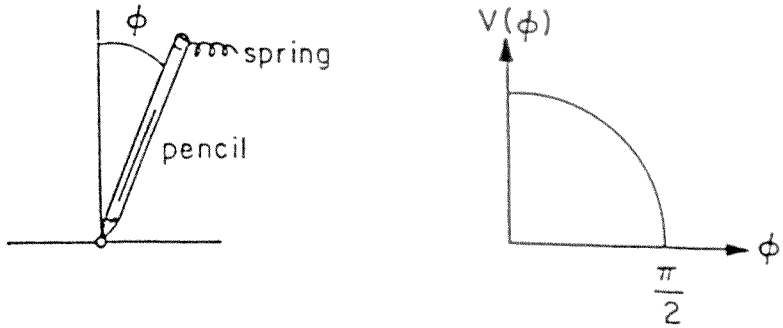

Fig. 16. The pencil model: the potential energy of a simple pencil has the same form as that of scalar fields used for spontaneous symmetry breaking. The springs connecting nearest neighbor pencils give rise to contributions to the energy which mimic spatial gradient terms in field theory.

At high temperatures $T \gg T_c$, all pencils undergo large amplitude high frequency oscillations. However, by causality, the phases of oscillation of pencils with large separation s are uncorrelated. For a system in thermal equilibrium, the length s beyond which phases are random is the correlation length $\xi(t)$. By causality there is an *a priori* causality bound on ξ:

$$\xi(t_c) < t_c\,, \tag{4.1}$$

where t_c is the causal horizon, at temperature T_c.

The critical temperature T_c is the temperature at which the thermal energy is equal to the energy a pencil needs to jump from a horizontal to a vertical position. For $T < T_c$, all pencils want to lie flat on the table. However, their orientations are random beyond a distance of $\xi(t_c)$.

The boundaries between the domains of correlated orientation become topological defects. Hence, it follows from the above causality argument that during the phase transition a network of defects with mean separation $\xi(t) \leq t$ will form.

For models of structure formation and for defects formed in grand unified phase transitions, we are interested in models with a scale of symmetry breaking $\eta \sim 10^{16}$ GeV corresponding to a time of formation $t_c \sim 10^{-35}$ sec.

which scales like the background radiation density. Later in this section we shal see that the scaling (4.13) does indeed hold in the cosmic string model. Hence cosmic strings do not lead to cosmological problems. On the contrary, since fo GUT models with $\eta \sim 10^{16}$ GeV

$$\frac{\rho_{cs}}{\rho_c} \sim \left(\frac{\eta}{m_{Pl}}\right)^2 \sim 10^{-6}, \tag{4.14}$$

cosmic strings in these models could provide the seed perturbations responsible fo structure formation.

Theories with local monopoles are ruled out on cosmological grounds[77] (see agai the caveats of Refs. 70 and 71) for rather different reasons. Since there are no lon range forces between local monopoles, their number density in comoving coordinate does not decrease. Since their contribution to the energy density scales as $a^{-3}(t)$ they will come to dominate the mass of the Universe, provided η is sufficiently large

Theories with global monopoles[78] are not ruled out, since there are long rang forces between monopoles which lead to a "scaling solution" with a fixed numbe of monopoles per Hubble volume.

4.3. *Cosmic string evolution*

Applied to cosmic strings, the Kibble mechanism implies that at the time of th phase transition, a network of cosmic strings with typical step length $\xi(t_G)$ wi form. According to numerical simulations,[79] about 80% of the initial energy is i infinite strings and 20% in closed loops.

The evolution of the cosmic string network for $t > t_G$ is complicated. The ke processes are loop production by intersections of infinite strings (see Fig. 17) an loop shrinking by gravitational radiation. These two processes combine to create mechanism by which the infinite string network loses energy (and length as measure in comoving coordinates). It will be shown that, as a consequence, the correlatio length of the string network is always proportional to its causality limit:

$$\xi(t) \sim t. \tag{4.15}$$

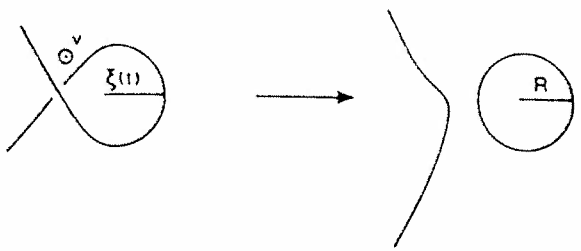

Fig. 17. Formation of loops by self-intersection of infinite strings. According to the original cosm string scenario, loops form with radius R determined by the instantaneous correlation length the infinite string network.

Hence, the energy density $\rho_\infty(t)$ in long strings is a fixed fraction of the background energy density $\rho_c(t)$:

$$\rho_\infty(t) \sim \mu\xi(t)^{-2} \sim \mu t^{-2} \tag{4.16}$$

or

$$\frac{\rho_\infty(t)}{\rho_c(t)} \sim G\mu. \tag{4.17}$$

We conclude that the cosmic string network approaches a "scaling solution"[80] in which the statistical properties of the network are time-independent if all distances are scaled to the horizon distance.

The origin of the scaling solution for the infinite string network can be understood heuristically, as follows. If the curvature radius $\xi(t)$ of this network is much larger than the Hubble radius t, the network will be frozen in comoving coordinates (since the Hubble damping term dominates in the equations of motion). Hence in the radiation-dominated FRW epoch

$$\xi(t) \sim a(t) \sim t^{1/2} \tag{4.18}$$

and the Hubble radius will catch up to $\xi(t)$. Conversely, if $\xi(t) \ll t$ then the tension term in the equations of motion for the string will dominate, the strings will oscillate relativistically and there will be frequent self-intersections of the strings, leading to rapid loop production and to increasing $\xi(t)/t$. Combining these two arguments, we conclude that there must be a "dynamical fixed point" with $\xi(t) \sim t$.

A first step in a more rigorous analysis of cosmic string evolution is the derivation of the effective equation of motion for the strings. Note that this equation must follow from the field equations since the string is merely a particular topologically stable field configuration.

The equations of motion of a string can be derived from the Nambu action

$$S = -\mu \int d\sigma\, d\tau \left(-\det g^{(2)}_{ab}\right)^{1/2}, \quad a, b = 0, 1, \tag{4.19}$$

$g^{(2)}_{ab}$ is the world-sheet metric and σ and τ are the world-sheet coordinates. In flat space–time, τ can be taken to be coordinate time, and σ is an affine parameter along the string. In terms of the string coordinates $X^\mu(\sigma, \tau)$ and the metric $g^{(4)}_{\mu\nu}$ of the background space–time,

$$g^{(2)}_{ab} = X^\mu_{,a} X^\nu_{,b} g^{(4)}_{\mu\nu}. \tag{4.20}$$

From general symmetry considerations, it is possible to argue that the Nambu action is the correct action. However, I shall follow Foerster[81] and Turok[82] and give a direct heuristic derivation. We start from a general quantum field theory Lagrangian, $\mathcal{L}_{QFT}$. The action is

$$S = \int d^4y\, \mathcal{L}_{QFT}(\phi(y)). \tag{4.21}$$

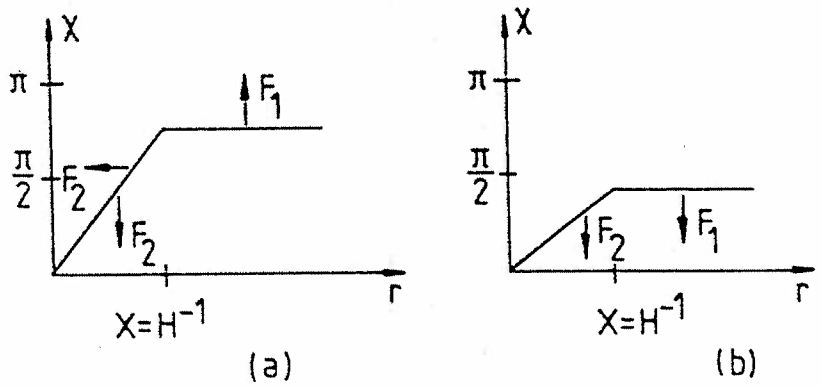

Fig. 18. A sketch of the forces acting on a radially symmetric texture configuration and which cause unwinding in Fig. 18(a) if $n_w > n_c$, and dissipation if $n_w < n_c$ [Fig. 18(b)].

However, for $\chi_{max} < \pi/2$, the angular gradient force tends to reduce χ_{max}, and to reduce the radial gradients, $\chi(r)$ will tend to decrease even for $\chi < \chi_{max}$. Hence, the field configuration will dissipate [see Fig. 18(b)].

If n_w is only slightly larger than $\pi/2$, the force F_1 of Fig. 15(a) is too weak to offset the force F_2 described above. The critical winding n_c is hence larger than 0.5. The precise value has been determined in Refs. 99 and 101. It depends on the length of the "plateau region" of $\chi(r)$ (which is the inter-texture separation) and on the expansion rate of the Universe. For realistic parameters[101]

$$0.65 < n_c < 0.75 . \tag{4.56}$$

As will be shown in a later section, only textures with $n_w > n_c$ generate localized density perturbations which can act as seeds for cosmic structure formation.

5. Introduction to Structure Formation

5.1. *Power spectrum*

In Sec. 2, the cosmology of a homogeneous and isotropic Universe was reviewed. In order to understand structure formation, it is essential to study the evolution of inhomogeneities at a linearized level. This will be adequate for understanding the early evolution of density perturbations in the Universe.

The starting point of the relativistic theory of cosmological perturbations[103] is the linearized Einstein equations. If we take the general Einstein equations

$$G_{\mu\nu} = 8\pi G T_{\mu\nu} , \tag{5.1}$$

where $G_{\mu\nu}(g_{\alpha\beta})$ is the Einstein tensor and $T_{\mu\nu}$ is the energy–momentum tensor of matter, and expand about a cosmological background solution

$$g_{\mu\nu}{}^{(0)} = \mathrm{diag}\,(1, -a^2(t), -a^2(t), -a^2(t)) \tag{5.2}$$

and

$$T^{\mu(0)}_{\nu} = \mathrm{diag}\,(\rho, -p, -p, -p) \tag{5.3}$$

(see Sec. 2), then we obtain the linearized equations

$$\delta G_{\mu\nu}\left(g_{\alpha\beta}{}^{(0)} + h_{\alpha\beta}\right) = 8\pi G \delta T_{\mu\nu} . \tag{5.4}$$

Equation (5.4) relates the perturbation $h_{\mu\nu}$ of the metric, i.e.

$$h_{\mu\nu} = g_{\mu\nu} - g_{\mu\nu}{}^{(0)} , \tag{5.5}$$

to the matter perturbations.

To gain a heuristic understanding of how the perturbations evolve, recall that gravity is a purely attractive force. Given an initial mass perturbation δm, the force on surrounding particles will be

$$F \sim \delta m . \tag{5.6}$$

Since (neglecting for a moment the expansion of the Universe)

$$\delta \ddot{m} \sim F , \tag{5.7}$$

we see that in a nonexpanding background the growth of perturbations is exponential. In an expanding background, there will be a damping term depending on H. Hence, perturbations will increase only as a power of time.

The details of the analysis are rather complicated (see Refs. 30 and 104 for recent reviews). The result is that the density contrast $\delta\rho$ grows as follows:

$$\delta\rho(t) \sim \begin{cases} t^{2/3} & t > t_{eq} \\ t & t < t_{eq} , \quad \lambda > t \\ \mathrm{const} & t < t_{eq} , \quad \lambda < t . \end{cases} \tag{5.8}$$

Note that on length scales λ greater than the Hubble radius t, the quantity $\delta\rho$ is not gauge-invariant, i.e. it depends on the slicing of space–time.[104] The quantity which is gauge-invariant is the relativistic potential Φ, which is time-independent if the equation of state of the background cosmology is constant.[104] In a gauge in which $g_{\mu\nu}$ is diagonal and for models of matter in which δT_{ij} is diagonal at linearized level (a condition satisfied by most interesting models of matter), Φ can be identified as follows:

$$g_{\mu\nu} = (1 + 2\Phi)dt^2 - a^2(t)(1 - 2\Phi)d\underline{x}^2 . \tag{5.9}$$

We will use the results of (5.8) when describing the evolution of the power spectrum.

The main quantity of interest is the r.m.s. mass excess $(\delta M/M)(k,t)$ at time t in a sphere of radius k^{-1}. Given a smooth density distribution

$$\rho(\underline{x}, t) = \rho_0(t) + \delta\rho(\underline{x}, t) , \tag{5.10}$$

the r.m.s. mass excess can be related to the Fourier mode $\delta\rho(k)$ in a straightforward manner.[18] The result is

$$\left(\frac{\delta M}{M}\right)^2(k,t) \simeq k^3\left|\frac{\delta\rho}{\rho_0}\right|^2(k,t)\,. \tag{5.11}$$

The adopted convention for Fourier transformation is

$$\delta\rho(\underline{x}) = (2\pi)^{-3/2}V^{-1/2}\int d^3k\, e^{i\underline{k}\underline{x}}\delta\rho(\underline{k})\,. \tag{5.12}$$

The result (5.11) holds provided $|\delta\rho(k)|^2$ is proportional to k^n with $n > -3$. An intuitive way to understand the result is as follows: perturbations with wave number larger than k average to zero in a volume k^{-3}, perturbations with wave number smaller then k are phase-space-suppressed such that $(\delta M/M)(k)$ receives its major contribution from Fourier modes of wave number k. Their phase space volume is k^3.

The most commonly used function describing the ensemble of perturbations is the spectrum $P(k)$. By definition, the power spectrum is the square of the modulus of the Fourier space density contrast:

$$P(k) = \left|\frac{\delta\rho}{\rho_0}(k)\right|^2. \tag{5.13}$$

Hence [from (5.11)], $P(k)$ is related to the r.m.s. mass fluctuations $(\delta M/M)(k,t)$ on physical length scale

$$\lambda_k = a(t)\frac{2\pi}{k} \tag{5.14}$$

at time t via

$$\left(\frac{\delta M}{M}\right)^2(k,t) \simeq k^3P(k)\,. \tag{5.15}$$

The scaling solution for topological defect models implies that when measured at the time $t_H(k)$ at which the wavelength λ_k equals the Hubble radius, the r.m.s. mass perturbation $(\delta M/M)(k)$ is independent of k (scale invariant), i.e.

$$\frac{\delta M}{M}(k, t_H(k)) = \text{const}\,. \tag{5.16}$$

This is because at any time t, a constant fraction of the mass M inside the Hubble radius is contained in the topological defects. For example, one cosmic string of length t contains mass $\delta M = \mu t$ compared to the total mass $M \sim t^3\rho(t) \sim t$ inside the Hubble radius, thus leaving the ratio $\delta M/M$ time-independent.

Equation (5.16) is the same result as is obtained for inflationary Universe models. Hence, we conclude that all three main models of structure formation — adiabatic random phase perturbations from inflation, cosmic strings, and global textures — to a first approximation produce a scale-invariant spectrum.

To convert (5.16) into an expression for the power spectrum $P(k)$, we use the fact that $\delta M/M$ grows as the scale factor $a(t)$ during the matter-dominated epoch on scales smaller than the Hubble radius [see (5.8)]:

$$\frac{\delta M}{M}(k,t) = \left[\frac{t}{t_H(k)}\right]^{2/3}\frac{\delta M}{M}(k, t_H(k))\,. \tag{5.17}$$

On scales larger than the Hubble radius at t_{eq}

$$t_H(k) = 2\pi k^{-1}a(t_H(k)) \sim t_H^{2/3}(k)k^{-1}\,, \tag{5.18}$$

and hence

$$t_H(k) \sim k^{-3}\,. \tag{5.19}$$

Therefore, combining (5.16), (5.17) and (5.19) we obtain

$$\frac{\delta M}{M}(k,t) \sim k^2\,. \tag{5.20}$$

From (5.15) it follows that

$$P(k) \sim k^n \tag{5.21}$$

with $n = 1$.

Recently, there has been some interest in deviations from scale invariance. In models of inflation, a deviation comes about[105] because H decreases slowly during inflation. In topological defect models, numerical[106,107] and semianalytical[108] studies have also shown small deviations from scale invariance. These deviations, however, are all small and quite model-dependent.

5.2. *CMB anisotropies*

Density perturbations give rise to anisotropies in the temperature of the CMB. There are three main contributions (see Fig. 19):

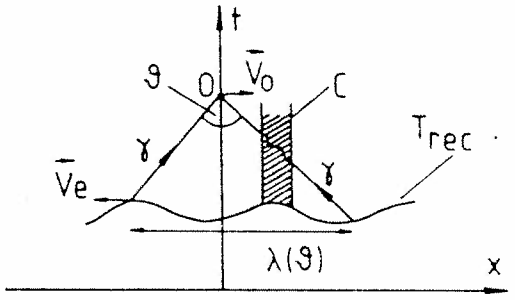

Fig. 19. Space–time plot sketching the origin of CMB temperature anisotropies. The surface labeled T_{rec} is the last scattering surface. O is the observer at the present time measuring photons γ impinging from directions in the sky separated by angle ϑ. The shaded area labeled C stands for a local overdensity, leading to distortions of geodesics. Possible velocities of observer and emitter are indicated as $\vec{v_o}$ and $\vec{v_e}$.

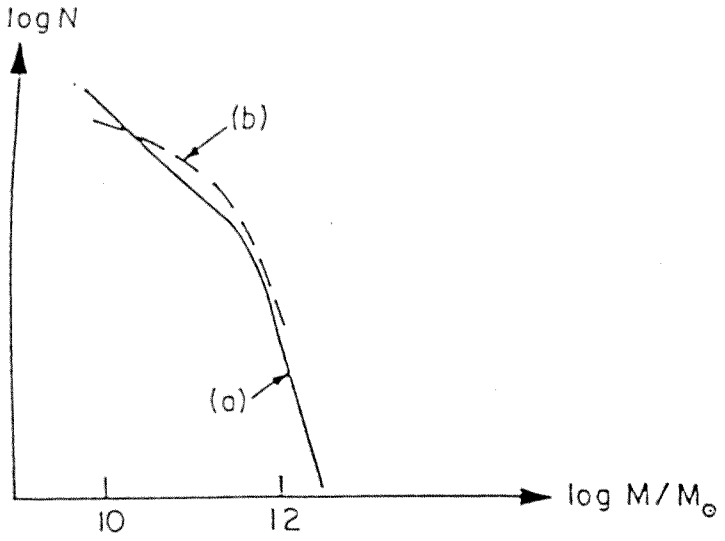

g. 22. The mass function of galaxies (determined from the luminosity function assuming constant ass to light ratio) from Ref. 127 [(a) from Bahcall, (b) from Binggeli].

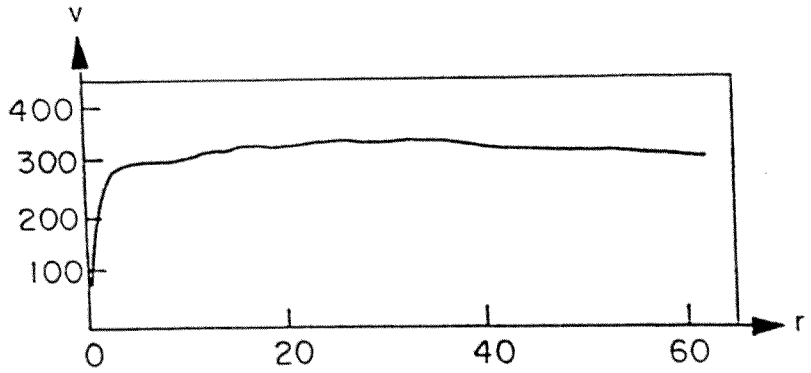

ig. 23. A typical velocity rotation curve (for NGC488 HI data, taken from Ref. 128). The radius in kpc, the velocity in km s^{-1}.

$$\rho(r) \sim r^{-2} . \tag{5.30}$$

We can also measure the angular momentum of galaxies. Typical numbers for large pirals are in the range[129] 10^{73}–10^{75} cm^{2}g s^{-1}.

. Cosmic Strings and Structure Formation

The starting point of the structure formation scenario in the cosmic string theory is he scaling solution for the cosmic string network, according to which at all times t in particular at t_{eq}, the time when perturbations can start to grow) there will be a few long strings crossing each Hubble volume, plus a distribution of loops of radius $R \ll t$ (see Fig. 24).

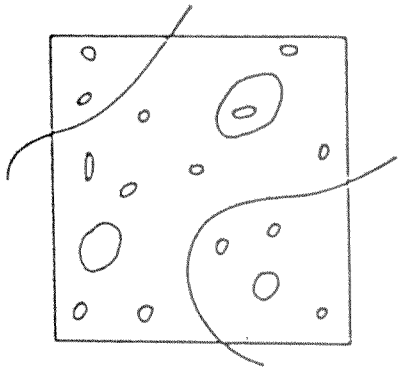

Fig. 24. Sketch of the scaling solution for the cosmic string network. The box corresponds to one Hubble volume at arbitrary time t.

The cosmic string model admits three mechanisms for structure formation: loops, filaments and wakes. Cosmic string loops have the same time-averaged field as a point source with mass[130]

$$M(R) = \beta R \mu , \tag{6.1}$$

R being the loop radius and $\beta \sim 2\pi$. Hence, loops will be seeds for spherical accretion of dust and radiation.[80]

For loops with $R \leq t_{eq}$, growth of perturbations in a model dominated by cold dark matter starts at t_{eq}. Hence, the mass at the present time will be

$$M(R, t_0) = z(t_{eq}) \beta R \mu . \tag{6.2}$$

In the original cosmic string model[80,131] it was assumed that loops dominate over wakes. In this case, the theory could be normalized (i.e. μ could be determined) by demanding that loops with the mean separation of clusters d_{cl} [from the discussion in Subsec. 4.4 it follows that the loop radius $R(d_{cl})$ is determined by the mean separation] accrete the correct mass, i.e. that

$$M(R(d_{cl}), t_0) = 10^{14} M_\odot . \tag{6.3}$$

This condition yields[131]

$$\mu \simeq 10^{36} \text{ GeV}^2 . \tag{6.4}$$

Thus, if cosmic strings are to be relevant for structure formation, they must arise due to symmetry breaking at energy scale $\eta \simeq 10^{16}$ GeV. This scale happens to be the scale of unification of weak, strong and electromagnetic interactions. It is tantalizing to speculate that cosmology is telling us that there indeed is new physics at the GUT scale.

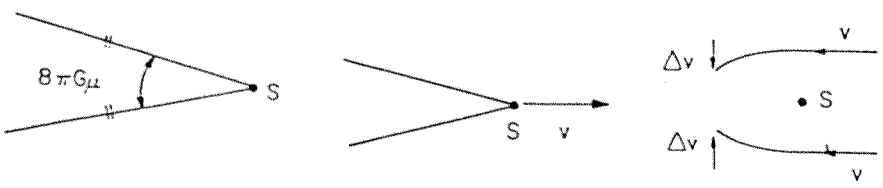

Fig. 25. Sketch of the mechanism by which a long straight cosmic string moving with velocity v in the transverse direction through a plasma induces a velocity perturbations Δv towards the wake. Shown on the left is the deficit angle, in the center is a sketch of the string moving in the plasma, and on the right is a sketch of how the plasma moves in the frame in which the string is at rest.

The second mechanism involves long strings moving with relativistic speed in their normal plane which give rise to velocity perturbations in their wake. The mechanism is illustrated in Fig. 25: space normal to the string is a cone with deficit angle[132]

$$\alpha = 8\pi G\mu \,. \tag{6.5}$$

If the string is moving with normal velocity v through a bath of dark matter, a velocity perturbation

$$\delta v = 4\pi G\mu v\gamma \tag{6.6}$$

[with $\gamma = (1 - v^2)^{-1/2}$] towards the plane behind the string results.[133] At times after $t_{\rm eq}$, this induces planar overdensities, the most prominent (i.e. thickest at the present time) and numerous of which were created at $t_{\rm eq}$, the time of equal matter and radiation.[134,135] The corresponding planar dimensions are (in comoving coordinates)

$$t_{\rm eq} z(t_{\rm eq}) \times t_{\rm eq} z(t_{\rm eq}) v \sim (40 \times 40 v)\ {\rm Mpc}^2 \,. \tag{6.7}$$

An intuitive understanding of the origin of the above distinguished scale can be obtained as follows. Viewed from a distance, the density perturbation grows as in a linear theory, i.e.

$$\frac{\delta\rho}{\rho}(t) = \left(\frac{t}{t_i}\right)^{2/3} \frac{\delta\rho}{\rho}(t_i) \,, \tag{6.8}$$

for a perturbation set up at a time $t_i > t_{\rm eq}$. Since the initial $\delta\rho/\rho(t_i)$ is independent of t_i, the largest density contrast comes from the earliest t_i, namely $t_i = t_{\rm eq}$. Fluctuations created at $t_i < t_{\rm eq}$ are erased by the large thermal velocities. Thus, strings at $t_{\rm eq}$ create the most prominent wakes. They are also the must numerous, since the comoving separation of strings decreases as t_i decreases.

A more rigorous way to obtain the above result is to consider the evolution of the velocity perturbations induced by a wake in the Zel'dovich approximation.[30] The height of a dark matter particle above the wake can be written as

where q is the initial comoving distance, and $\psi(q,t)$ is the comoving displacement caused by the presence of the wake. The thickness of the wake at time t is determined by the value of q for which

$$\dot{h}(q,t) = 0 \,. \tag{6.10}$$

Obviously, the value of q for which $\dot{h} = 0$ increases as the time when the perturbation ψ begins to grow is moved back in time. Hence, the earliest wakes will be the thickest.

The details of the calculation depend on whether the dark matter is hot or cold (see Sec. 8). For hot dark matter, the large thermal velocities delay the beginning of the growth of ψ on small scales. A detailed analysis[136,137] shows that for hot dark matter no perturbations become nonlinear unless

$$G\mu > 5 \cdot 10^{-7} \,. \tag{6.11}$$

In this case, the value of the redshift $z(q)$ at which $\dot{h} = 0$ is maximal for the value of q (the thickness) given by

$$q \sim G\mu v\gamma(v) z(t_{\rm eq})^2 t_{\rm eq} \sim 4v\ {\rm Mpc} \tag{6.12}$$

for wakes created at $t_i = t_{\rm eq}$. Note that the scales of cosmic string wakes [see (6.7) and (6.12)] compare favorably with the measures of the observed sheets of galaxies.[9]

Wakes arise if there is little small scale structure on the string. In this case, the string tension equals the mass density, the string moves at relativistic speeds, and there is no local gravitational attraction towards the string.

In contrast, if there is small scale structure on strings, then[95] the string tension T is smaller than the mass per unit length μ and the metric of a string in the z direction becomes

$$ds^2 = (1 + h_{00})[dt^2 - dz^2 - dr^2 - (1 - 8G\mu) r^2 d\theta^2] \tag{6.13}$$

with

$$h_{00} = 4G(\mu - T) \ln \frac{r}{r_0} \,, \tag{6.14}$$

r_0 being the string width. Since h_{00} does not vanish, there is a gravitational force towards the string which gives rise to cylindrical accretion, thus producing filaments.

As is evident from the last term in the metric (6.13), space perpendicular to the string remains conical, with the deficit angle given by (6.5). However, since the string is no longer relativistic, the transverse velocities v of the string network are expected to be smaller, and hence the induced wakes will be shorter.

Which of the mechanisms — filaments or wakes — dominates is determined by the competition between the velocity induced by h_{00} and the velocity perturbation of the wake. The total velocity is[138,139]

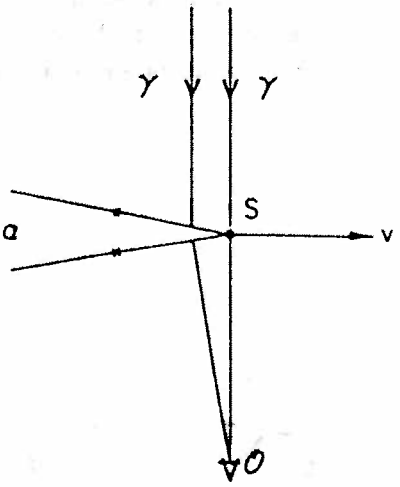

Fig. 31. Sketch of the mechanism producing linear discontinuities in the microwave temperature for photons γ passing on different sides of a moving string S (velocity v). O is the observer. Space perpendicular to the string is conical (deficit angle α).

$$\frac{\delta T}{T} \sim 8\pi G\mu v\gamma(v)\,. \tag{8.6}$$

To detect such discontinuities, an appropriate survey strategy (for example, a full sky survey) with small angular resolution is crucial. The distribution of strings also gives rise to Sachs–Wolfe type anisotropies.[155]

The theoretical error bars in the normalization of CMB anisotropies from strings are rather large — a direct consequence of the fact that the precise form of the scaling solution for the string network is not well determined. Nevertheless, we can consider a fixed set of cosmic string parameters and ask whether the normalizations of $G\mu$ from large scale structure data and from COBE are consistent. This has been done numerically in Ref. 106, and using an analytical toy model in Ref. 108.

The analytical model[108] is based on adding up as a random walk the individual Doppler shifts from strings which the microwave photons separated by angular scale v pass on different sides, and using this method to compute $\Delta T/T(\theta)$. By the use of the Bennett–Bouchet[156] string parameters, the result for $G\mu$ becomes

$$G\mu = (1.3 \pm 0.5)10^{-6}\,, \tag{8.7}$$

in good agreement with the requirements from large scale structure formation.[7]

To detect the predicted anisotropies from textures, it is again essential to have a full sky survey. However, larger angular resolution is adequate this time, since the specific signature for textures is a small number ($\sim$ 10) of hot and cold disks with amplitude[157]

$$\frac{\delta T}{T} \sim 0.06 \times 16\pi G\eta^2 \sim 3 \cdot 10^{-5} \tag{8.8}$$